SENSITIVITY OF THE MICROBUNCHING INSTABILITY TO IRREGULARITIES IN CATHODE CURRENT IN THE LCLS-II BEAM DELIVERY SYSTEM*

C. Mitchell†, J. Qiang, M. Venturini, LBNL, Berkeley, CA 94720, USA
P. Emma, SLAC, Menlo Park, CA 94025, USA

Abstract

LCLS-II is a high-repetition rate (1 MHz) Free Electron Laser (FEL) X-ray light source now under construction at SLAC National Accelerator Laboratory. During transport to the FEL undulators, the electron beam is subject to a space charge-driven microbunching instability that can degrade the electron beam quality and lower the FEL performance if left uncontrolled. The present LCLS-II design is well-optimized to control the growth of this instability out of the electron beam shot noise. However, the instability may also be seeded by irregularities in the beam current profile at the cathode (due to non-uniformities in the temporal profile of the photogun drive laser pulse). In this paper, we describe the sensitivity of the microbunching instability to small-amplitude temporal modulations on the emitted beam current profile at the cathode, using high-resolution simulations of the LCLS-II beam delivery system.

INTRODUCTION

The microbunching instability plays a significant role in the dynamics of electron beam transport for 4th generation light sources, and much of the LCLS-II design effort [1] has been devoted to understanding microbunching phenomena seeded by the electron beam shot noise in the LCLS-II beam delivery system [2]. The present LCLS-II design has been well-optimized to control these effects through careful tuning of the local momentum compaction of the lattice [3], but irregularities in the temporal profile of the emitted bunch current at the photocathode may also seed the instability [4], originating from non-uniformities of the photocathode drive laser pulse (if the beam is generated using a single pulse) or pulse-to-pulse variations of drive laser power (if the beam is generated through longitudinal stacking).

Table 1 describes the nominal 100 pC beam that is used in this study. The nominal emitted current profile is uniform along the bunch, with linear rise and fall over a 2 ps interval at either end. We investigate the effect of adding a small-amplitude modulation to the initial current profile, so that the bunch current is described by ($\chi << 1$):

$$I(t) = I_0(1 + \chi \cos(2\pi t/\tau)), \quad \tau \in [1, 9]\ \text{ps}. \qquad (1)$$

All simulations are performed using the IMPACT code suite [5, 6], and begin with initialization of the electron beam at the photocathode. To correctly resolve the beam shot noise, we use a number of simulation particles equal to the number of electrons in the physical bunch (625M), with a grid resolution of $64 \times 64 \times 2048$.

Table 1: Parameters describing the nominal 100 pC beam used for single-bunch cathode-undulator tracking. Final values are provided at the entrance to the first hard X-ray FEL undulator.

Parameter	Value
Bunch charge	100 pC
Transverse beam size at the cathode (rms)	0.192 mm
Thermal emittance at the cathode (rms)	1 μm/mm
Initial bunch duration (FWHM)	33 ps
Final kinetic energy	4.1 GeV
Final peak current (beam core)	714 A
Final slice emittance $\epsilon_{x,n}$ (rms, beam core)	0.48 μm
Final slice emittance $\epsilon_{y,n}$ (rms, beam core)	0.38 μm
Final slice energy spread (rms, beam core)	562 keV

MICROBUNCHING IN THE PHOTOINJECTOR

Figure 1 illustrates the amplitudes of the density and energy modulations present on the bunch at the exit of the first cryomodule (~100 MeV). The results are quite linear in the amplitude of the cathode-applied modulation up to $\chi = 5 - 10\%$. The results using 5M and 625M simulation particles are similar, suggesting that the applied modulation dominates the effect of shot-noise seeded microbunching in this region. Ballistic compression in the photoinjector system is expected to contribute to enhanced spatial bunching [4]. However, simulations indicate that any short-wavelength density modulation present on the bunch at the first RF cavity entrance is damped rapidly during acceleration, reappearing as increased modulation in the bunch slice energy profile.

Adiabatic Phase Damping of Plasma Oscillations

The transformation of modulations from density profile to energy profile during acceleration is closely related to the phenomenon of adiabatic synchrotron phase damping, and can be understood as follows. We model microbunching in the cryomodule using the integral equations in [7], assuming

* Work supported by the U.S. Department of Energy under Contract Nos. DE-AC02-76SF00515, DE-AC02-05CH11231, and the LCLS-II Project.
† ChadMitchell@lbl.gov

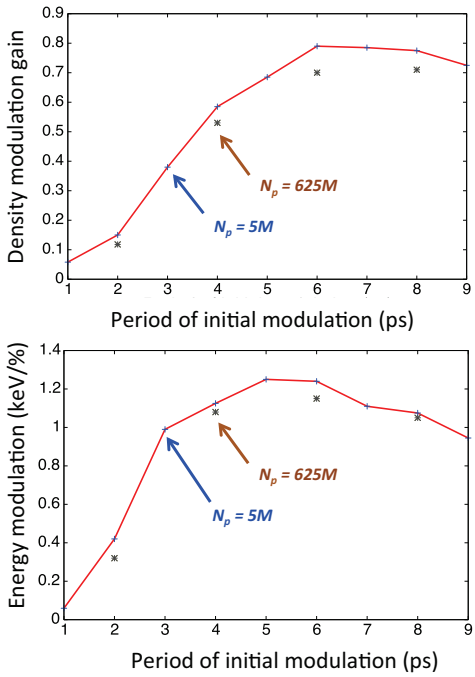

Figure 1: Density (upper) and energy (lower) modulation amplitudes at the exit of the injector cryomodule, shown as a function of the period τ of the modulation applied at the photocathode. Both quantities are normalized by the amplitude χ of the applied modulation.

acceleration on-crest for simplicity:

$$b(k,s) = b(k,0) + \int_0^s K(\tau,s)b(k,\tau)d\tau, \tag{2a}$$

$$\Delta\gamma(k,s) = \Delta\gamma(k,0) - \frac{I}{I_A}\int_0^s \frac{4\pi Z(k,\tau)}{Z_0}b(k,\tau)d\tau, \tag{2b}$$

where Z is an appropriate longitudinal space charge impedance [8]. (See [9] for a treatment of RF compression.) We consider the case when $\Delta\gamma(k,0) = 0$. Here

$$K(\tau,s) = 4\pi i\frac{I}{I_A}k\frac{Z(k,\tau)}{Z_0}\int_\tau^s \frac{ds'}{\gamma(s')^3}. \tag{3}$$

Setting $Z_\infty = iZ_0/\pi k r_b^2$, where $r_b \approx 2\sigma_x$ is the beam radius, it is convenient define the dimensionless real quantities:

$$u = -i\Delta\gamma, \quad \tilde{Z}(k,s) = \frac{Z(k,s)}{Z_\infty(k,s)}. \tag{4}$$

The integral equations (2) can then be expressed as a Hamiltonian system in the variables (b,u) described by:

$$H(b,u;s) = \frac{k}{2\gamma(s)^3}u^2 + \frac{2}{kr_b(s)^2}\frac{I}{I_A}\tilde{Z}(k,s)b^2. \tag{5}$$

In the limit when (5) varies slowly over a plasma period, the quantities b and u each undergo plasma oscillations whose amplitudes are described by the adiabatically-varying envelopes:

$$|b|_{\max}(s) = |b_0|\sqrt{\frac{r_b(s)}{r_{b0}}}\left(\frac{\gamma_0}{\gamma(s)}\right)^{\frac{3}{4}}\left[\frac{\tilde{Z}(k,0)}{\tilde{Z}(k,s)}\right]^{\frac{1}{4}}, \tag{6}$$

$$|\Delta\gamma|_{\max}(s) = \frac{2|b_0|}{k\sqrt{r_{b0}r_b(s)}}\sqrt{\frac{I}{I_A}}[\gamma_0\gamma(s)]^{\frac{3}{4}}\left[\tilde{Z}(k,0)\tilde{Z}(k,s)\right]^{\frac{1}{4}},$$

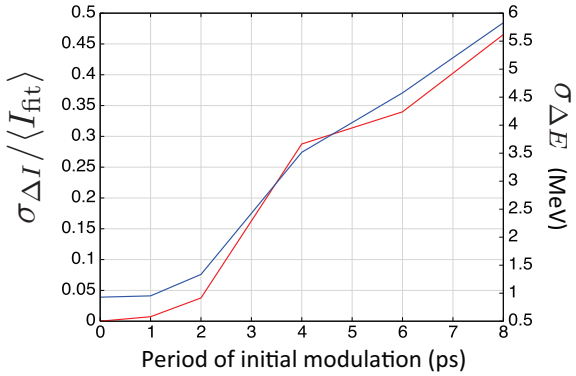

Figure 2: Microbunching diagnostics at the HXR undulator for particles within a window [-10,10] μm containing the beam core (χ = 5%). (Red) Relative rms current fluctuation about the unmodulated current profile. (Blue) Projected energy spread after removing the unmodulated mean slice energy of each longitudinal slice.

where b_0 is the bunching factor at the cryomodule entrance. This gives an approximate scaling of the energy modulation amplitude at the cryomodule exit as $\sim \gamma^{3/4}\sigma_x^{-1/2}\lambda$. Using the simulated beam parameters at the cryomodule entrance, (6) predicts an energy modulation at the injector exit of 1.4 keV, reasonably near the simulated value of 1.6 keV.

MICROBUNCHING IN THE LINAC AND TRANSPORT LINES

During propagation through the first magnetic bunch compressor (R_{56} = −58.1 mm), energy modulations emerging from the injector are mapped into density modulations that seed additional microbunching in the linac, the first dogleg, and the bypass line. Figure 2 illustrates the final microbunching present on the beam at the HXR undulator for a modulation of amplitude χ = 5% at the cathode. Here, bunching in the beam current profile is measured by taking the rms value of $\Delta I = I - I_{\rm fit}$ over an interval [-10,10] μm surrounding the beam core, where $I_{\rm fit}$ is the current of the nominal (unmodulated) beam. Likewise, the projected rms energy spread of particles within the interval [-10,10] μm is computed after taking $\Delta E = E - E_{\rm fit}$ for each particle, where $E_{\rm fit}$ is the mean energy in the corresponding longitudinal slice of the nominal beam.

The microbunching on the final beam increases quickly with modulation period τ for $\tau \geq 2$ ps. Figures 3-4 illustrate the beam longitudinal phase space at the HXR undulator for several cases of interest. The bunching structure also has an impact on the horizontal projected beam emittance growth, as illustrated in Fig. 5. This is due to the presence of large current spikes in the beam current profile, which lead to enhanced CSR-induced emittance growth in the bends of the two bunch compressors and the final dogleg.

CONCLUSION

Cathode-to-undulator tracking of the LCLS-II beam delivery system with self-consistent, 3D space charge was per-

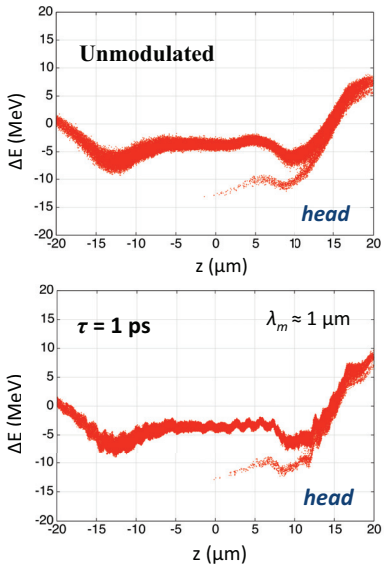

Figure 3: (Upper) Longitudinal phase space at the HXR undulator for a nominal 100 pC beam with no applied modulation ($\chi = 0$). (Lower) Longitudinal phase space at the HXR undulator for the case $\chi = 5\%$, $\tau = 1$ ps.

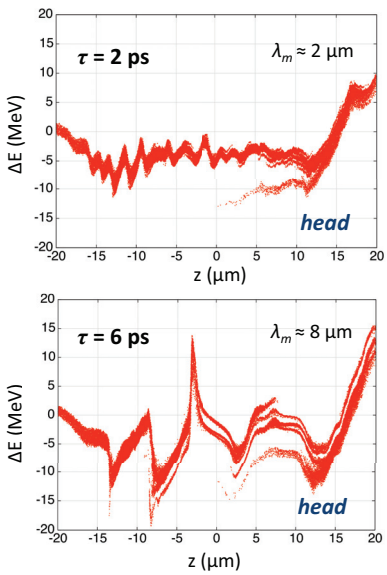

Figure 4: (Upper) Longitudinal phase space at the HXR undulator for the case $\chi = 5\%$, $\tau = 2$ ps. (Lower) Longitudinal phase space at the HXR undulator for the case $\chi = 5\%$, $\tau = 6$ ps.

formed using the physical number of particles in the beam, after applying a modulation to the initial beam profile, to study the combined effects of shot-noise seeded and cathode noise-seeded microbunching. The presence of irregularity in the temporal profile of the beam at the cathode introduces structure in the beam current profile and longitudinal phase space at the HXR undulator, primarily at wavelengths > 1 μm. This effect is most problematic for spectral components at the cathode with periods $\tau > 2$ ps. To keep current modulation at the undulator within a few %, current modulations at the cathode at periods longer than 2 ps should

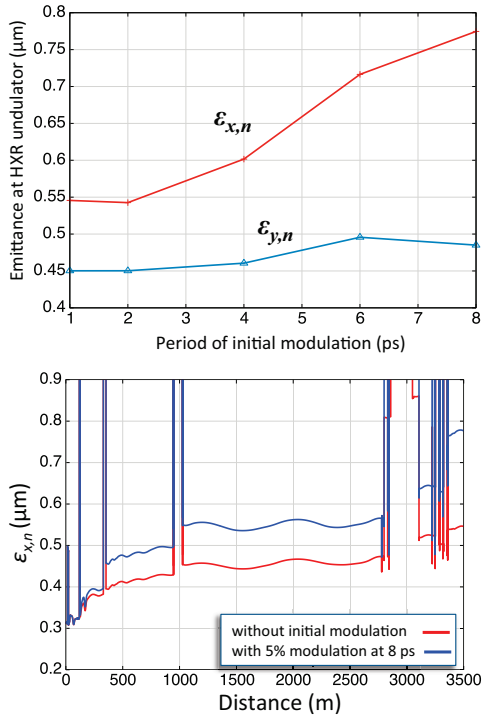

Figure 5: (Upper) Projected emittance at the HXR undulator for the case $\chi = 5\%$, shown for several values of applied modulation period τ. (Lower) Comparison of the horizontal emittance evolution of the nominal beam and the case $\chi = 5\%$, $\tau = 8$ ps, illustrating CSR-induced emittance growth.

be controlled well within 5 %. Significant CSR-induced horizontal emittance growth (> 10%) can also occur in the presence of initial current modulations with period > 4 ps.

ACKNOWLEDGMENT

This work is supported by the Office of Science of the U.S. Department of Energy under Contract Numbers DE-AC02-76SF00515, DE-AC02-05CH11231, and the LCLS-II Project, and made use of computer resources at the National Energy Research Scientific Computing Center.

REFERENCES

[1] T. Raubenheimer, in *Proc. FEL'2015*, pp. 618-624.

[2] M. Venturini, in *Proc. FEL'2015*, pp. 308–316.

[3] J. Qiang *et al.*, in *Proc. IPAC'2016*, pp. 1695–1698.

[4] J. Qiang *et al.*, in *Proc. IPAC'2013*, p. 1709.

[5] J. Qiang *et al.*, *J. Comp. Phys.*, vol. 163, pp. 434-451, 2000.

[6] J. Qiang, S. Lidia, and R. Ryne, *Phys. Rev. ST Accel. Beams*, vol. 9, p. 044204, 2006.

[7] C. Limborg-Deprey, P. Emma, Z. Huang, and J. Wu, in *Proc. EPAC'2004*, pp. 1506–1608.

[8] J. Qiang, R. Ryne, M. Venturini, A. Zholents, and I. Pogorelov, *Phys. Rev. ST Accel. Beams*, vol. 12, p. 100702, 2009.

[9] M. Venturini *et al.*, *Phys. Rev. ST Accel. Beams*, vol. 13, p. 080703, 2010.